Molecular Catalysis 514 (2021) 111840

Contents lists available at ScienceDirect

Molecular Catalysis

journal homepage: www.journals.elsevier.com/molecular-catalysis

Theoretical studies about C_2H_2 semi-hydrogenation on the carbon material supported metal cluster catalysts: Influences of support type and cluster size on the catalytic performance

Yamin Qi [a,b], Xiuxiu Shao [a,b], Baojun Wang [a,b], Lixia Ling [a,b], Riguang Zhang [a,b,*]

[a] State Key Laboratory of Clean and Efficient Coal Utilization, Taiyuan University of Technology, Taiyuan 030024, Shanxi, PR China
[b] Key Laboratory of Coal Science and Technology (Taiyuan University of Technology), Ministry of Education, PR China

ARTICLE INFO

Keywords:
C_2H_2 semi-hydrogenation
Carbon material supports
Cluster sizes
Electronic properties analysis

ABSTRACT

The support type and cluster size of the supported catalysts strongly affect their catalytic performance toward the targeted reaction. This study is designed to investigate the influences of support type and cluster size on C_2H_4 selectivity and activity of C_2H_2 semi-hydrogenation; density functional theory calculations were utilized to illustrate C_2H_2 semi-hydrogenation mechanism on the catalysts with the different carbon material supported different sizes of metal clusters. The results show that for the different carbon material supported single-atom Cu or Pd catalysts, the support types greatly affect C_2H_4 selectivity and activity, among them, GDY support shows excellent catalytic performance. On the other side, as to the M_n/GDY (M=Cu, Pd) catalysts with different cluster sizes, the activity of Pd_n/GDY is generally better than that of Cu_n/GDY; while the selectivity of Cu_n/GDY is better than that of Pd_n/GDY. Interestingly, Pd_1/GDY presents excellent C_2H_4 selectivity and activity for C_2H_2 semi-hydrogenation, attributing to its moderate Mulliken charge of metal atoms. This study could provide valuable structure clue for the obtaining of highly-efficient supported catalysts with suitable carbon material support and cluster size.

1. Introduction

Acetylene (C_2H_2) semi-hydrogenation to ethylene (C_2H_4) has been widely applied to purify C_2H_4 stream in the industry [1-3]. Pd catalysts are industrially used for C_2H_2 semi-hydrogenation due to its high activity, while it exhibits low C_2H_4 selectivity [4, 5]. Further, Pd alloyed the second metal Cu [6], Ag [7], or Au [8] are used to improve C_2H_4 selectivity, while the high cost of Pd limits its widespread use.

Nowadays, great attention has been attracted about the single-atom catalysts (SACs) in terms of heterogeneous catalysis field due to its unusual catalytic properties, maximized atom utilization, unique electronic and geometric structures [9-11]. Importantly, the strong metal-support interaction plays a vital role in providing an ideal platform for anchoring active center and optimizing the electronic and geometric structures of metal atoms [12, 13]. Thus, choosing appropriate support material is of great significance. In recent years, the high specific surface area and the unique physical and chemical properties make carbon material as the support well improve the catalytic performance. For instance, the experiment found that Pd_1/N-graphene exhibited 99% C_2H_2 conversion and 93.5% C_2H_4 selectivity [14]. Experimental studies by Huang *et al.* [15] showed that Cu_1/ND@G (G=grephene) catalyst achieved 95% C_2H_2 conversion, 98% C_2H_4 selectivity and more than 60 h stability; meanwhile, DFT studies indicated that C_2H_4 desorption priority resulted in high C_2H_4 selectivity on Cu_1/ND@G. The experimental and theoretical studies demonstrated that Co_1/G showed excellent activity and selectivity for azoxy aromatic compounds in nitroarenes hydrogenation [16]. Pd_1/graphene exhibited high selectivity toward 1-butene in 1,3-butadiene hydrogenation [17]. Pd_1/graphene catalyst has nearly 100% butene selectivity and 95% 1, 3-butadiene conversion in 1,3-butadiene hydrogenation [18]. Above results showed that the graphene supported single-atom catalysts unveil better catalytic performance for selective hydrogenation reaction.

Extensive work has revealed that the defects on graphene affect the physical and chemical properties of graphene [19-22]. Graphene with single- and double-defects shows outstanding ability to anchor single-atom Fe [23]. Besides the defects on graphene, the moderate additive into carbon material is also a practical method to advance the catalytic performance. Both experimental and theoretical studies

* Corresponding author.
E-mail address: zhangriguang@tyut.edu.cn (R. Zhang).

https://doi.org/10.1016/j.mcat.2021.111840
Received 16 May 2021; Received in revised form 4 August 2021; Accepted 17 August 2021
Available online 29 August 2021

demonstrated that the B-doped and N-doped graphene had better catalytic performance, for example, the experiments elucidated that B-doped graphene is a valid electrocatalyst for hydrogenation evolution reaction [24]. Interestingly, the theoretical studies revealed that B-doped graphene was reactive enough to chemically bind NO_2 and NO [25]. Pt_1/N-C exhibits superior performance for the hydrogenation among twenty-four SACs [26]. The Cu-N_3 site of Cu-SA/HCNS experimentally shows an 86% benzene conversion and 96.7% phenol selectivity in benzene selective oxidation to phenol [27].

Further, nitrogenized holey doped graphene (g-C_2N and g-C_3N_4) have been synthesized and attracted a lot of attention. Fe_1Cu_1@C_2N processes better CO oxidation activity [28]. C_2N-Co^{2+} facilitated HCOOH dehydrogenation via decreasing the rate-determining barrier [29]. The calculations showed that M_1/g-C_3N_4 was highly selective for propane dehydrogenation, especially the single-atom V, Cr, Mn anchored on g-C_3N_4 [30]. Pd_1/C_3N_4 single-atom catalyst has better C_2H_4 selectivity and coking resistance for C_2H_2 hydrogenation [31]. Pd_1/g-C_3N_4 exhibits high selectivity but low activity energy in C_2H_2 semi-hydrogenation, which also agrees with the experiments [32]. Interestingly, graphdiyne (GDY), as a new type of carbon material, shows good prospects for industrial applications, for example, Lu *et al.* [33] investigated a series of M/GDY catalysts, Rh and Ir with low concentrations (about 1.37 at%) have the potential to be applied as single metal catalysts. DFT studies found that $M_xM'_{3-x}$/GDY (M, M'=Ru, Os) catalysts have high C_2H_4 selectivity in C_2H_2 semi-hydrogenation [34]. Meanwhile, both C_2H_4 selectivity and activity greatly depend on the composition and size of Pd_xM_y/GDY (M=Cu, Ag, Au, Ni; x+y=1-3) catalysts [35].

On the other side, in the supported metal cluster catalyst, the sizes of metal cluster affect the reactive performance. DFT calculations showed that Fe_2 clusters exhibited superior activity for acidic oxygen reduction reaction among Fe_x(x=1-3) clusters on N-doped grapheme [36]. Among Au_x(x=3, 4, 5, 6, 7, 13, 38) clusters, small planar clusters are more active for a series of Lewis acid and oxidation reactions [37]. The Gibbs free energy of HCOOH dehydrogenation on Ni_x@C_2N(x=1-3) predicted that Ni_2@C_2N exhibits excellent catalytic activity [38]. Kuo *et al.* [39] showed that Pt nanoparticles in the subnanometer size regime exhibits remarkably high selectivity to C_2H_4 compared to the low selectivity on the large Pt nanoparticles. The theoretical studies by Ma *et al.* [40] studied C_2H_2 semi-hydrogenation over the oxygen-defected anatase TiO_2(110) (Ana-Ov) supported Pt cluster (n=1, 2, 4, 8) catalysts, indicating that the adsorption strength of C_2H_2 and C_2H_4 increases with the increasing of Pt cluster size, implying the higher catalytic activity is possible. Shi *et al.* [41] elucidated that the decreasing of Cu particle size reduces the activity considerably, however, both C_2H_4 selectivity and durability in C_2H_2 semi-hydrogenation were gradually improved; Cu SAC exhibited the highest C_2H_4 selectivity of 91% at the complete conversion along with excellent long-term stability for at least 40 h, whereas the rapid deactivation occurred on Cu nanoparticle catalysts.

Reports in the above literatures, however, vary widely, and the catalytic performance of various carbon material supported metal single-atom or clusters for C_2H_2 semi-hydrogenation remains elusive. Several carbon materials, such as single-defect graphene, double-defect graphene, B-doped graphene, N-doped graphene, g-C_2N, g-C_3N_4 and GDY, supported single-atom and metal cluster catalysts to exhibit better catalytic performance in selective hydrogenation reactions. However, for C_2H_2 semi-hydrogenation, the influence of carbon material type on the catalytic performance is still unclear. Meanwhile, when carbon material is the same, the influence of supported metal cluster sizes on the catalytic performance is also unknown. Thus, it is necessary to clarify what type of the support and what size of the cluster may be the most suitable for C_2H_2 semi-hydrogenation.

This study is designed to identify the influences of support type and cluster size on the catalytic performance of the carbon material supported metal cluster catalysts for C_2H_2 semi-hydrogenation, DFT calculation method is used to systematically study the activity and selectivity of C_2H_2 semi-hydrogenation on different types of carbon material supported metal cluster with different sizes. Carbon materials mainly focus on single-defect graphene, double-defect graphene, B-doped graphene, N-doped graphene, g-C_2N, g-C_3N_4 and GDY; metal clusters mainly consider different sizes of Cu and Pd clusters. The results are expected to obtain the most suitable carbon support type and cluster size for C_2H_2 semi-hydrogenation, which can provide a reference structure clues for screening and designing catalysts with excellent catalytic performance in C_2H_2 semi-hydrogenation.

2. Computational details

2.1. Computational method

The Dmol^3 code was used to carry out DFT calculations [42, 43]. The exchange-correlation was illustrated by generalized gradient approximation (GGA) realized by Predew-Burke-Ernzerhof (PBE) functional [44]. Considering the dispersion effect, DFT-D corrections was employed to describe the van der walls interaction [45-47]. A $3 \times 3 \times 1$ k-point was set in the structure optimization and other relevant computations. The double numerical basis set plus polarization function (DNP) was utilized to treat the valence electron wave function [48]. The complete LST/QST method was used to search the transition state [49], TS Confirmation and frequency analysis methods were used to confirm the transition state.

2.2. Computational models

In order to illustrate the influence of support type in the carbon material supported metal catalysts, the single-defect graphene, double-defect graphene, B-doped graphene, N_1-doped graphene, N_2-doped graphene, N_3-doped graphene, g-C_2N, g-C_3N_4 and GDY are considered to support single-atom M (M=Cu or Pd), there are eighteen kinds of catalysts, donated as M_1/SVG, M_1/DVG, M_1/BVG, M_1/NVG, M_1/N_2VG, M_1/N_3VG, M_1/C_2N, M_1/C_3N_4, M_1/GDY.

On the other hand, aiming at identifying the influence of cluster size in the carbon material supported metal cluster catalysts, GDY is considered to support different sizes of metal M (M=Cu or Pd) cluster catalysts, there are fourteen kinds of catalysts, donated as M_2/GDY, M_3/GDY, M_4/GDY, M_7/GDY, M_{13}/GDY, M_{38}/GDY, M_{55}/GDY. All optimized catalyst structures are shown in Fig. 1.

2.3. The stability of various carbon material supported metal cluster catalysts

The stability of all catalysts is evaluated by the calculation of the binding energy between the metal clusters and carbon material supports. The binding energy (E_b) is defined as follows:

$$E_b = E_{cluster/support} - E_{support} - E_{cluster} \quad (1)$$

Where $E_{cluster/support}$, $E_{support}$ and $E_{cluster}$ stand for the total energy of the $M_{cluster}$/support system, the support and the metal cluster, respectively. The more negative the binding energy is, the more stable the catalyst is. As listed in Table 1, the binding energy is below -300 kJ•mol^{-1}, indicating that the carbon material supported metal cluster catalysts is extremely stable.

2.4. Free energy calculation

All the adsorption and reaction energies involved in this study were calculated at a finite temperature to consider the entropy and thermal contribution.

The adsorption free energy (G_{ads}) is calculated by the Eq. (2):

$$G_{ads} = E_{surface} + G_{surface} + E_{adsorbate} + G_{adsorbate} - E_{system} - G_{system} \quad (2)$$

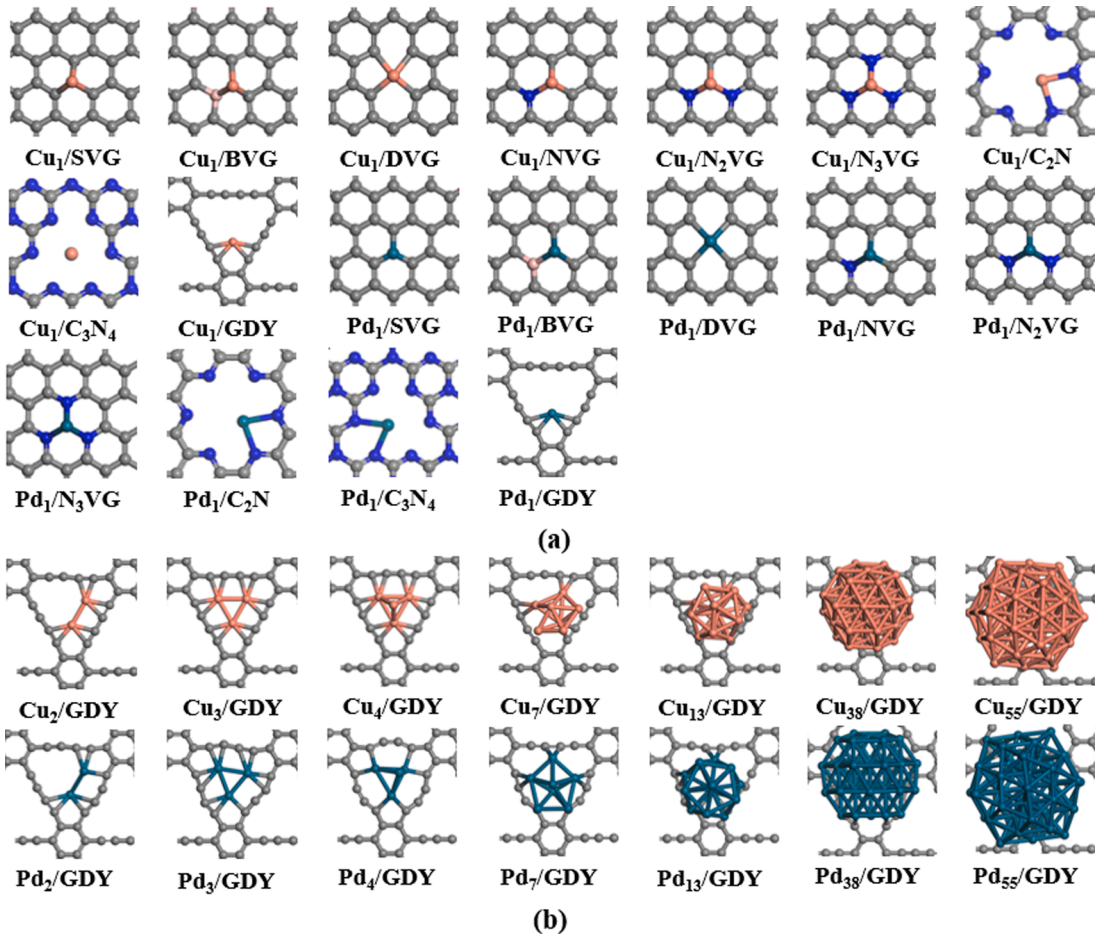

Fig. 1. The structures of different carbon material supported M_n (M=Cu, Pd, n=1, 2, 3, 4, 7, 13, 38, 55) catalysts. (a) The supported single-atom M (M=Cu, Pd) catalysts; (b) The supported cluster M_n (M=Cu, Pd, n=2, 3, 4, 7, 13, 38, 55) catalysts.

Table 1
The binding energy (E_b/kJ•mol^{-1}) between the carbon material and the supported M_n (M=Cu, Pd, n=1, 2, 3, 4, 7, 13, 38, 55) cluster.

Catalysts	E_b/kJ•mol^{-1}	Catalysts	E_b/kJ•mol^{-1}
Cu_1/SVG	-568.8	Pd_1/SVG	-747.3
Cu_1/BVG	-389.0	Pd_1/BVG	-543.4
Cu_1/DVG	-713.4	Pd_1/DVG	-685.4
Cu_1/NVG	-491.0	Pd_1/NVG	-565.7
Cu_1/N_2VG	-523.4	Pd_1/N_2VG	-560.1
Cu_1/N_3VG	-490.2	Pd_1/N_3VG	-438.3
Cu_1/C_2N	-523.3	Pd_1/C_2N	-510.4
Cu_1/C_3N_4	-379.9	Pd_1/C_3N_4	-330.9
Cu_1/GDY	-434.9	Pd_1/GDY	-481.2
Cu_2/GDY	-441.3	Pd_2/GDY	-608.9
Cu_3/GDY	-652.1	Pd_3/GDY	-636.1
Cu_4/GDY	-696.0	Pd_4/GDY	-653.0
Cu_7/GDY	-555.9	Pd_7/GDY	-759.6
Cu_{13}/GDY	-776.2	Pd_{13}/GDY	-924.1
Cu_{38}/GDY	-1253.2	Pd_{38}/GDY	-1742.9
Cu_{55}/GDY	-1480.9	Pd_{55}/GDY	-2244.7

Where $E_{surface}$ is the total energy of the clean catalyst surface, $E_{adsorbate}$ is the total energy of the gas-phase adsorbate, and E_{system} is the total energy of adsorbate-substrate system in its equilibrium state; $G_{surface}$, $G_{adsorbate}$ and G_{system} are the corresponding free energies corrections at a finite temperature. Based on the above definition, the more negative the value of G_{ads} is, and the stronger the adsorption ability of the adsorbed species on the surface is.

Activation free energy (G_a) and reaction free energy (ΔG) are calculated on the basis of the Eqs. (3) and (4) at a finite temperature.

$$G_a = E_{TS} + G_{TS} - E_{IS} - G_{IS} \quad (3)$$

$$\Delta G = E_{FS} + G_{FS} - E_{IS} - G_{IS} \quad (4)$$

Where E_{IS}, E_{TS} and E_{FS} stand for the total energies of initial state (IS), transition state (TS) and final state (FS), respectively; G_{IS}, G_{TS} and G_{FS} correspond to the corrections of the free energies at a finite temperature. The DMol^3 output document of frequency analysis can directly obtain the values of G_{IS}, G_{TS} and G_{FS}.

3. Results and discussion

3.1. Paths of C_2H_2 semi-hydrogenation

As illustrated in Fig. 2, C_2H_2 hydrogenation not only generates gaseous C_2H_4, but also forms ethane due to C_2H_4 over-hydrogenation. Thus, three paths exist: C_2H_2+H→C_2H_3+H→C_2H_4 (C_2H_4 desorption path), C_2H_2+H→C_2H_3+H→C_2H_4+2H→ C_2H_6 (C_2H_4 intermediate path)

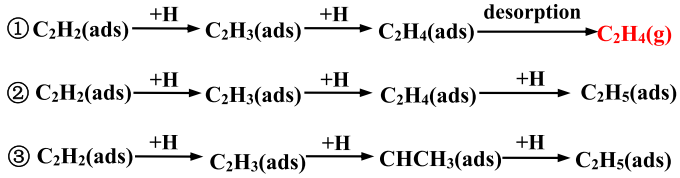

Fig. 2. Possible reactions of C_2H_2 semi-hydrogenation. (ads) and (g) stand for the adsorbed and gaseous states, respectively.

and C_2H_2+H→C_2H_3+H→$CHCH_3$+2H→C_2H_6 ($CHCH_3$ intermediate path).

C_2H_2 selective hydrogenation on the Cu-based catalysts occurs at the temperature of 423~523 K [50, 51] and Pd-based catalysts usually occurs at the temperature of 300~500 K under the experimental conditions [52, 53]. On the other hand, "green oil" is generated by the polymerization process, which makes the catalysts deactivation [54, 55], and previous studies found that the accumulation of green oil results in the decreasing of hydrogenation activity at low temperature [56, 57]. Meanwhile, the higher H_2/C_2H_2 ratio of 10: 1 is beneficial to suppress the formation of green oil and inhibit the irreversible deactivation of the catalyst [58, 59]. Thus, the high temperature and H_2/C_2H_2 ratio are beneficial to prevent green oil formation. H_2/C_2H_2 ratio of 10:1 and the temperature 425 K are chosen and the "green oil" formation is not considered in this work. Since C_2H_2 content in the raw C_2H_4 is only 0.1 to 1%, C_2H_4 content is high as 89%, and the experimental pressure is the standard pressure [5, 60-61], correspondingly, 0.01, 0.1 and 0.89 atm are the partial pressures of C_2H_2, H_2 and C_2H_4, respectively.

3.2. C_2H_2 and C_2H_4 adsorption

The produced C_2H_4 contains 0.1~1% of C_2H_2 in the steam-cracking process, removing trace C_2H_2 in the raw C_2H_4 can be achieved when C_2H_2 adsorption is stronger than C_2H_4 [62]. Fig. S1 and Table 2 present the most stable configurations of C_2H_2 and C_2H_4 on the carbon material supported metal M (M=Cu, Pd) catalysts and its corresponding adsorption free energies at 425 K.

For eighteen kinds of carbon material supported single-atom M catalysts, see Table 2, both C_2H_2 and C_2H_4 are weakly adsorbed (19.9 and 32.2 kJ•mol^{-1}) on Cu_1-DVG; C_2H_2 adsorption is weaker than C_2H_4 adsorption (-34.8 and -36.1 kJ•mol^{-1}) on Pd_1-C$_2$N. However, on other sixteen kinds of the catalysts, Cu_1/SVG, Cu_1/BVG, Cu_1/NVG, Cu_1/N_2VG, Cu_1/N_3VG, Cu_1/C_2N, Cu_1/C_3N_4, Cu_1/GDY, Pd_1/SVG, Pd_1/BVG, Pd_1/DVG, Pd_1/NVG, Pd_1/N_2VG, Pd_1/N_3VG, Pd_1/C_3N_4 and Pd_1/GDY, C_2H_2 adsorption is stronger than C_2H_4 adsorption, trace C_2H_2 can be adsorbed on the catalysts for C_2H_2 subsequent hydrogenation.

For fourteen kinds of GDY supported metal M cluster catalysts, see Table 2, C_2H_2 adsorption is still stronger than C_2H_4 adsorption, namely, trace C_2H_2 can be adsorbed on the catalysts for C_2H_2 subsequent hydrogenation.

Table 2
The adsorption free energies (G_{ads}/kJ•mol^{-1}) of C_2H_2 and C_2H_4 species on the different carbon material supported M_n (M=Cu, Pd, n=1, 2, 3, 4, 7, 13, 38, 55) catalysts.

Catalysts	G_{ads} C_2H_2	C_2H_4	Catalysts	G_{ads} C_2H_2	C_2H_4
Cu_1/SVG	-98.0	-79.3	Pd_1/SVG	-44.6	-39.1
Cu_1/BVG	-99.8	-89.7	Pd_1-BVG	-51.6	-48.8
Cu_1/DVG	19.9	32.2	Pd_1-DVG	-84.3	-42.4
Cu_1/NVG	-95.2	-77.1	Pd_1-NVG	-95.6	-78.8
Cu_1/N_2VG	-103.2	-93.7	Pd_1-N_2VG	-145.2	-123.2
Cu_1/N_3VG	-144.0	-132.9	Pd_1-N_3VG	-143.4	-122.5
Cu_1/C_2N	-75.9	-69.1	Pd_1/C_2N	-34.8	-36.1
Cu_1/C_3N_4	-76.3	-35.9	Pd_1/C_3N_4	-104.0	-83.2
Cu_1/GDY	-96.1	-69.6	Pd_1/GDY	-63.4	-53.9
Cu_2/GDY	-134.3	-66.9	Pd_2/GDY	-117.5	-108.1
Cu_3/GDY	-27.5	-17.6	Pd_3/GDY	-205.2	-153.1
Cu_4/GDY	-75.5	-80.2	Pd_4/GDY	-177.8	-116.7
Cu_7/GDY	-225.9	-98.8	Pd_7/GDY	-185.5	-80.7
Cu_{13}/GDY	-171.7	-74.6	Pd_{13}/GDY	-204.0	-99.4
Cu_{38}/GDY	-125.4	-49.1	Pd_{38}/GDY	-272.3	-94.9
Cu_{55}/GDY	-125.2	-37.8	Pd_{55}/GDY	-246.0	-153.2

3.3. C_2H_2 hydrogenation on the supported M (M=Cu, Pd) single-atom catalysts

3.3.1. C_2H_4 desorption and its hydrogenation

As depicted in Fig 3 and Table S1, among above sixteen kinds of supported M single-atom catalysts, the reaction of C_2H_4+H→C_2H_5 is more favorable than C_2H_4 desorption in kinetics on five kinds of Cu_1/BVG (85.9 *vs.* 89.7 kJ•mol^{-1}), Cu_1/N_3VG (61.2 *vs.* 132.9 kJ•mol^{-1}), Pd_1/NVG (56.0 *vs.* 78.8 kJ•mol^{-1}), Pd_1/N_2VG (90.5 *vs.* 123.2 kJ•mol^{-1}) and Pd_1/N_3VG catalysts (95.7 *vs.* 122.5 kJ•mol^{-1}), namely, the adsorbed C_2H_4 is difficult to desorb from the catalyst and subjected to over-hydrogenation to ethane. However, C_2H_4 desorption is more kinetically superior to its hydrogenation C_2H_4+H→C_2H_5 on eleven kinds of Cu_1/SVG (80.6 *vs.* 79.3 kJ•mol^{-1}), Cu_1/NVG (120.1 *vs.* 77.1 kJ•mol^{-1}), Cu_1/N_2VG (100.6 vs. 93.7 kJ•mol^{-1}), Cu_1/C_2N (241.6 *vs.* 69.1 kJ•mol^{-1}), Cu_1/C_3N_4 (193.8 *vs.* 35.9 kJ•mol^{-1}), Cu_1/GDY (81.9 *vs.* 69.6 kJ•mol^{-1}), Pd_1/SVG (69.0 *vs.* 39.1 kJ•mol^{-1}), Pd_1/BVG (139.8 *vs.* 48.8 kJ•mol^{-1}), Pd_1/DVG (68.8 *vs.* 42.4 kJ•mol^{-1}), Pd_1/C_3N_4 (99.9 *vs.* 83.2 kJ•mol^{-1}) and Pd_1/GDY (330.9 *vs.* 53.9 kJ•mol^{-1}), namely, the adsorbed C_2H_4 is easy to desorb from these eleven catalysts to generate gaseous C_2H_4.

3.3.2. C_2H_2 semi-hydrogenation

As mentioned above, eleven kinds of supported single-atom M catalysts are screened out to favor C_2H_4 desorption to gaseous C_2H_4, thus, C_2H_2 hydrogenation is further examined on the Cu_1/SVG, Cu_1/NVG, Cu_1/N_2VG, Cu_1/C_2N, Cu_1/C_3N_4, Cu_1/GDY, Pd_1/SVG, Pd_1/BVG, Pd_1/DVG, Pd_1/C_3N_4 and Pd_1/GDY.

As to the supported single-atom Cu catalysts, on Cu_1/GDY, as shown in Fig. 4 and Table S2, the first step C_2H_2+H→C_2H_3 has an activation free energy of 34.0 kJ•mol^{-1} and reaction free energy of 123.5 kJ•mol^{-1}. Beginning with C_2H_3 intermediate, C_2H_4 formation is more kinetically favorable than $CHCH_3$ formation (90.9 *vs.* 105.0 kJ•mol^{-1}), namely, C_2H_2 hydrogenation can easily generate C_2H_4 intermediate, followed by its desorption to gaseous C_2H_4. Thus, Cu_1/GDY is more favorable to generate gaseous C_2H_4. Similar conditions appear on the Cu_1/C_2N (Fig. S3) and Cu_1/C_3N_4 (Fig. S4).

Interestingly, on Cu_1/SVG (see Fig. S5), the first step C_2H_2+H→C_2H_3 has an activation free energy of 123.7 kJ•mol^{-1} and reaction free energy of 167.6 kJ•mol^{-1}, beginning with C_2H_3 intermediate, $CHCH_3$ formation is more kinetically favorable than C_2H_4 formation (93.2 *vs.* 260.4 kJ•mol^{-1}), C_2H_2 is easily hydrogenated to generate $CHCH_3$ intermediate, followed by hydrogenation to ethane. Thus, Cu_1/SVG catalyst is not conducive to gaseous C_2H_4 generation. Similarly, such condition also occurs on the Cu_1/NVG (Fig. S6), Cu_1/N_2VG (Fig. S7).

As to the supported single-atom Pd catalysts, on the Pd_1/GDY (Fig. 5), Pd_1/BVG (Fig. S8) and Pd_1/C_3N_4 (Fig. S9), gaseous C_2H_4 generation is the most favored. However, on the Pd_1/SVG (Fig. S10) and Pd_1/DVG (Fig. S11), $CHCH_3$ formation is more favorable than C_2H_4 formation in kinetics, these two catalysts are conducive to ethane generation. Wang *et al.* [35] also demonstrated that Pd_1/GDY is in favor of C_2H_2 semi-hydrogenation to produce gaseous C_2H_4.

3.3.3. Influences of support types on the selectivity and activity of C_2H_4 formation

When C_2H_4 desorption path is more superior than other two hydrogenation paths in kinetics, the energy difference between C_2H_4 hydrogenation activation free energy ($G_{a,hydr}$) and C_2H_4 desorption free energy ($G_{a,des}$) is employed as a descriptor to qualitatively and quantitatively evaluate C_2H_4 selectivity, which is defined as follows:

$$S_{sel} = G_{a,hydr} - G_{a,des} \quad (5)$$

When $CHCH_3$ intermediate path is kinetically favorable than C_2H_4 desorption path, the difference of the overall activation free energy between the reactions C_2H_3+2H→C_2H_5 ($G_{hydr,CHCH3}$) and C_2H_3+H→C_2H_4 ($G_{hydr,C2H4}$) is used as a descriptor to evaluate C_2H_4

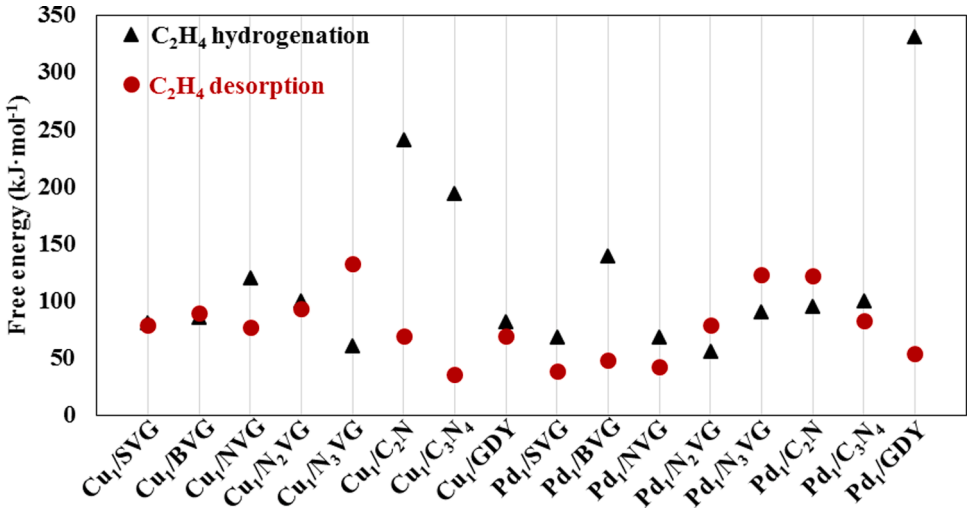

Fig. 3. C_2H_4 desorption free energy and its hydrogenation activation free energy on the different carbon material supported Cu and Pd single-atom catalysts.

selectivity, which is defined as follows:

$$S_{sel} = G_{hydr,CHCH3} - G_{hydr,C2H4} \quad (6)$$

When S_{sel} is positive, the catalyst shows good C_2H_4 selectivity, whereas it shows poor C_2H_4 selectivity. Meanwhile, two-step model is used to calculate C_2H_4 formation rate for evaluating catalytic activity (see details in the Supplementary Material).

C_2H_4 formation activity (r/molecules•s^{-1}•$site^{-1}$) is calculated using the Eq. (7):

$$r = \frac{k_B T}{h} = \frac{\left(1 - \frac{P_P}{P_R} e^{\frac{\Delta G}{RT}}\right)}{\frac{P^0}{P_R} e^{\frac{G_R^{ad} - G_R^{de} + G_P^{de}}{RT}} + e^{\frac{G_P^{de}}{RT}}} \quad (7)$$

Where T, P_R and P_P are the reaction temperature, the reactant partial pressure and the product partial pressure, respectively. According to the experimental conditions, P_R and P_P are set to be 0.11 and 0.89 atm, respectively; P^0 is the standard pressure, k_B and h are the Boltzmann constant and the Planck constant, respectively. ΔG is the overall reaction free energy of C_2H_2 semi-hydrogenation to C_2H_4, the obtained value from DFT calculations is -206.3 kJ•mol^{-1} at 425 K. G_R^{ad}, G_R^{de} and G_p^{de} can be obtained by the potential energy map of C_2H_2 semi-hydrogenation to C_2H_4

For carbon material supported single-atom Cu catalysts, as listed in Table 3, C_2H_4 selectivity on the Cu_1/C_2N, Cu_1/C_3N_4, Cu_1/GDY are 172.5, 157.9 and 12.3 kJ•mol^{-1}, C_2H_4 formation rates are 1.35×10^{-6}, 1.08×10^{-9} and 8.67×10^{3} molecules•s^{-1}•$site^{-1}$, respectively. However, C_2H_4 selectivity on the Cu_1/SVG, Cu_1/NVG, Cu_1/N_2VG are -167.2, -179.9 and -256.9 kJ•mol^{-1}, C_2H_4 formation rates are 5.54×10^{-3}, 7.67×10^{-4} and 3.77×10^{-32} molecules•s^{-1}•$site^{-1}$, respectively. C_2H_4 selectivity is in sequence of Cu_1/C_2N>Cu_1/C_3N_4>Cu_1/GDY>Cu_1/SVG>Cu_1/NVG>Cu_1/N_2VG, and the activity sequence of C_2H_4 formation is Cu_1/GDY>Cu_1/SVG>Cu_1/NVG> Cu_1/C_2N>Cu_1/C_3N_4>Cu_1/N_2VG. Thus, the Cu_1/C_2N, Cu_1/C_3N_4 and Cu_1/GDY favor C_2H_4 desorption path to generate gaseous C_2H_4, Cu_1/GDY shows poor C_2H_4 selectivity, but the best activity; whereas the Cu_1/C_2N and Cu_1/C_3N_4 exhibit poor activity of C_2H_4 formation, but the best C_2H_4 selectivity.

For carbon material supported single-atom Pd catalysts, C_2H_4 selectivity on the Pd_1/BVG, Pd_1/C_3N_4, Pd_1/GDY are 91.0, 16.7 and 277.0 kJ•mol^{-1}, C_2H_4 formation rates are 2.23×10^{0}, 1.66×10^{4} and 2.78×10^{9} molecules•s^{-1}•$site^{-1}$, respectively. However, C_2H_4 selectivity on the Pd_1/SVG and Pd_1/DVG are -89.2 and -153.9 kJ•mol^{-1}, C_2H_4 formation rates are 7.02×10^{7} and 7.35×10^{-3} molecules•s^{-1}•$site^{-1}$, respectively. C_2H_4 selectivity is in sequence of Pd_1/GDY>Pd_1/BVG>Pd_1/C_3N_4>Pd_1/SVG>Pd_1/DVG, and the activity order of C_2H_4 formation is Pd_1/GDY>Pd_1/SVG>Pd_1/C_3N_4>Pd_1/BVG> Pd_1/DVG. Thus, Pd_1/BVG, Pd_1/C_3N_4 and Pd_1/GDY catalysts are in favor of C_2H_4 desorption path to generate gaseous C_2H_4, Pd_1/GDY shows better gaseous C_2H_4 selectivity and activity than Pd_1/C_3N_4 and Pd_1/BVG.

Thus, six kinds of Cu_1/GDY, Cu_1/C_2N, Cu_1/C_3N_4, Pd_1/GDY, Pd_1/C_3N_4 and Pd_1/BVG are favorable to produce gaseous C_2H_4 with better catalytic performance.

3.3.4. *Electronic properties of the supported single-atom Cu and Pd catalysts*

Mulliken charge of metal atom on above six kinds of Cu_1/GDY, Cu_1/C_2N, Cu_1/C_3N_4, Pd_1/GDY, Pd_1/C_3N_4 and Pd_1/BVG catalysts is 0.015, 0.376, 0.423, 0.198, 0.131 and 0.222 *e*, respectively, suggesting that the electron transfer occurs from the metal atom to the support. As shown in Fig. 6, the relationship of Mulliken charge with C_2H_4 formation activity (lg$r$) shows a quasi-volcanic curve. Cu_1/GDY (0.015 *e*) and Pd_1/C_3N_4 (0.131 *e*) with less charge show poor activity of C_2H_4 formation (3.938 and 4.221 molecules•s^{-1}•$site^{-1}$); Pd_1/BVG (0.222 *e*) with more charge also exhibits the worst activity of C_2H_4 formation (0.349 molecules•s^{-1}•$site^{-1}$); Cu_1/C_2N and Cu_1/C_3N_4 catalysts with the most charge exhibits the worst activity of C_2H_4 formation (-5.870 and -8.967 molecules•s^{-1}•$site^{-1}$). However, Pd_1/GDY with moderate charge (0.198 *e*) exhibits the best activity of C_2H_4 formation (9.444 molecules•s^{-1}•$site^{-1}$). Similarly, for Pd_1/GDY catalyst, it also exhibits the best C_2H_4 selectivity (277.0 kJ•mol^{-1}) with the moderate charge of metal atom. Based on above analysis, the different support results in different electron transfer between the metal atom and the support, which alters the electronic properties of metal active center, and then affects the adsorption stability of reaction intermediates to exhibit an extremely different catalytic performance.

3.4. *C_2H_2 semi-hydrogenation on the M_n/GDY (M=Cu, Pd; n=2, 3, 4, 7, 13, 38, 55)*

Above results show that Pd_1/GDY exhibits excellent catalytic performance for C_2H_2 semi-hydrogenation. Meanwhile, Cu_1/GDY exhibits poor C_2H_4 selectivity and better C_2H_4 formation activity. Thus, the influence of cluster size on the catalytic performance of C_2H_2 semi-hydrogenation was further explored on fourteen kinds of the supported M_n/GDY (M=Cu, Pd; n=2, 3, 4, 7, 13, 38, 55) catalysts. C_2H_2 and C_2H_4 adsorption free energy and the stable configurations are shown in Table 2 and Fig. S1.

3.4.1. *C_2H_2 semi-hydrogenation*

For the supported Cu_n/GDY (n=2, 3, 4, 7, 13, 38, 55) catalysts, on

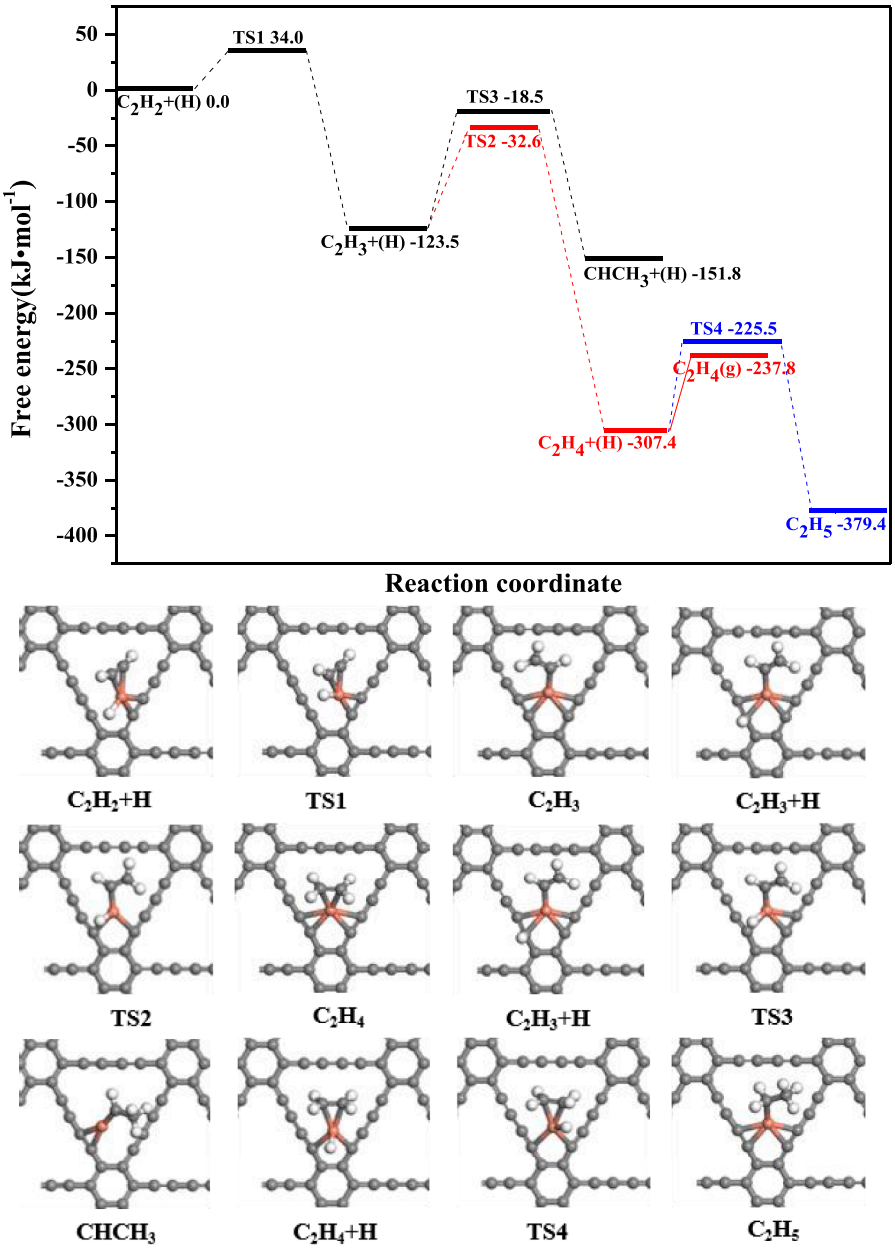

Fig. 4. Free energy profiles of C_2H_2 semi-hydrogenation with the initial states, transition states and final states on Cu_1/GDY catalyst.

Cu_2/GDY, Cu_3/GDY, Cu_7/GDY, Cu_{38}/GDY and Cu_{55}/GDY, see Figs. S13~S17, C_2H_4 desorption path exhibits more priority than other two paths, C_2H_4 selectivity is 115.9, 267.3, 64.3, 123.4 and 188.2 kJ•mol^{-1}, C_2H_4 formation rates are 2.61 × 10^{-1}, 6.89 × 10^{-12}, 1.81 × 10^{-18}, 3.42 × 10^{-14} and 6.73 × 10^{-11} molecules•s^{-1}•site^{-1}. Wang *et al.* [35] also showed that Cu_2/GDY and Cu_3/GDY are favorable for gaseous C_2H_4 formation. However, on the Cu_4/GDY and Cu_{13}/GDY, see Figs. S18 and S19, $CHCH_3$ intermediate path is the most favorable, C_2H_4 selectivity is -104.6 and -42.4 kJ•mol^{-1}, the rates are 1.81 × 10^{-10} and 1.51 × 10^{-20} molecules•s^{-1}•site^{-1}.

For the supported Pd_n/GDY (n=2, 3, 4, 7, 13, 38, 55) catalysts, on the Pd_4/GDY, Pd_7/GDY, Pd_{38}/GDY and Pd_{55}/GDY, see Figs. S20~S23, C_2H_4 desorption path is superior to other two paths with better C_2H_4 selectivity of 40.1, 57.8, 45.9 and 27.1 kJ•mol^{-1}, and C_2H_4 formation rates are 8.81 × 10^7, 2.91 × 10^{-1}, 5.23 × 10^{-14} and 1.43 × 10^{-9} molecules•s^{-1}•site^{-1}, respectively. However, on the Pd_2/GDY and Pd_3/GDY, see Figs. S24 and S25, C_2H_4 intermediate path is preferred in kinetics with poor C_2H_4 selectivity of -44.8 and -68.7 kJ•mol^{-1} and the rates of 1.20 × 10^8 and 1.23 × 10^{11} molecules•s^{-1}•site^{-1}. Meanwhile, Wang *et al.* [35] also elucidated that Pd_2/GDY and Pd_3/GDY catalysts are favorable for C_2H_4 intermediate path. On Pd_{13}/GDY, see Fig. S26, C_2H_2 hydrogenation is easy to form $CHCH_3$ and then successive hydrogenation to form ethane with poor C_2H_4 selectivity (-56.4 kJ•mol^{-1}) and C_2H_4 formation rate is 2.81 × 10^{-6} molecules•s^{-1}•site^{-1}.

3.4.2. Influences of cluster sizes on the selectivity and activity of C_2H_4 formation

As listed in Table 3, for the supported Cu_n/GDY catalysts, C_2H_4 selectivity is in sequence of Cu_3/GDY>Cu_{55}/GDY>Cu_{38}/GDY>Cu_2/GDY>Cu_7/GDY>Cu_1/GDY> Cu_{13}/GDY>Cu_4/GDY, and the activity order is Cu_1/GDY>Cu_2/GDY>Cu_4/GDY> Cu_{55}/GDY>Cu_3/GDY>Cu_{38}/GDY>Cu_7/GDY>Cu_{13}/GDY. C_2H_4 formation activity generally shows a decreased trend with the increase of cluster size; while C_2H_4 selectivity does not depend on the cluster sizes. Among them, Cu_1/GDY has better C_2H_4 selectivity (12.3 kJ•mol^{-1}) and the best activity (8.67 × 10^3 molecules•s^{-1}•site^{-1}); Cu_2/GDY has excellent C_2H_4 selectivity (115.9

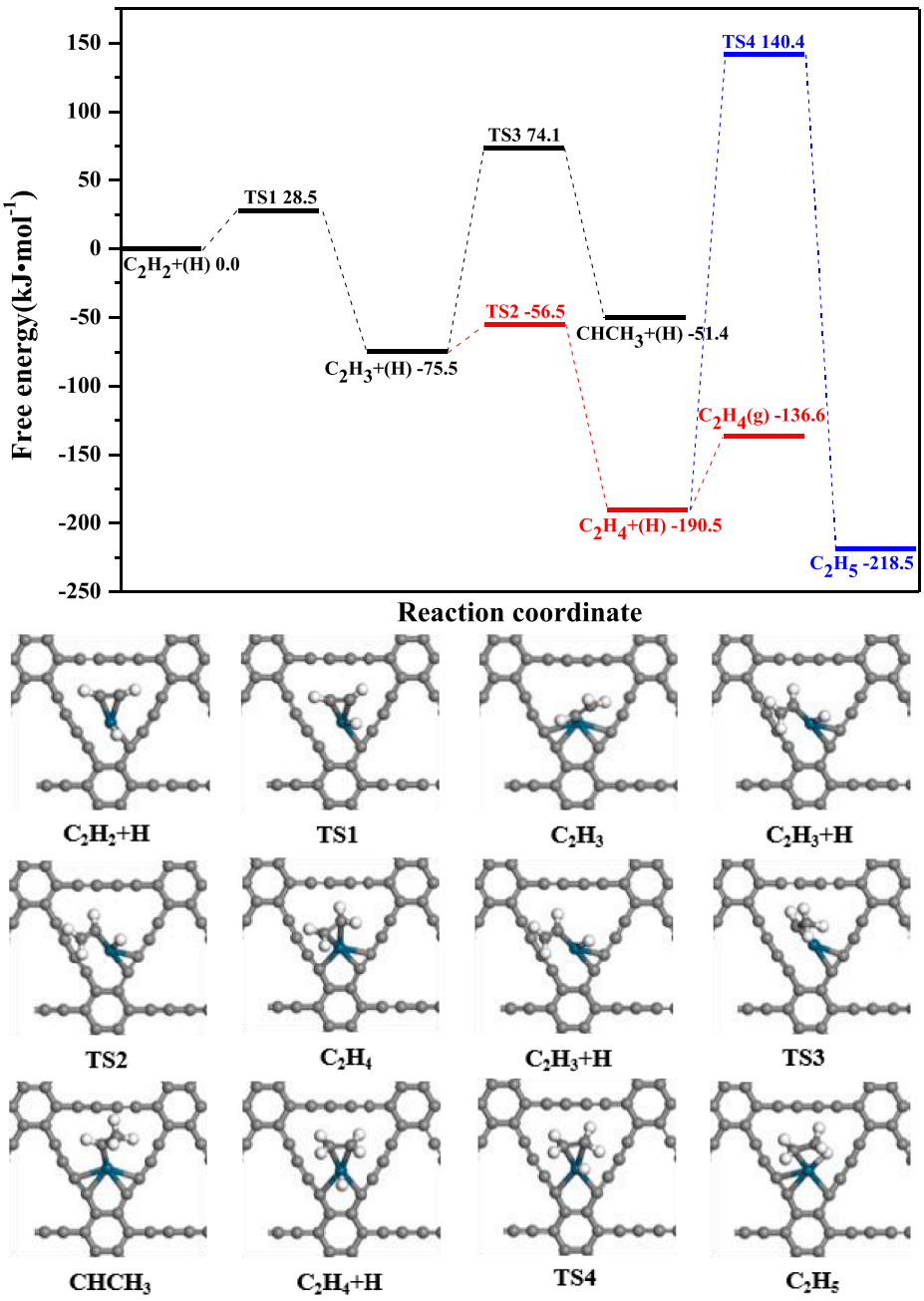

Fig. 5. Free energy profiles of C_2H_2 semi-hydrogenation with the initial states, transition states and final states on Pd_1/GDY catalyst.

Table 3
C_2H_4 selectivity (S_{sel}/kJ•mol^{-1}), its formation rate (r or lg$r$/molecules•s^{-1}•site^{-1}) on the different carbon material supported M_n (M=Cu, Pd, n=1, 2, 3, 4, 7, 13, 38, 55) catalysts at 425 K.

Catalysts	S_{sel}	r	lgr	Catalysts	S_{sel}	r	lgr
Cu_1/SVG	-167.2	5.54×10^{-3}	-2.257	—	—	—	—
Cu_1/NVG	-179.9	7.67×10^{-4}	-3.115	Pd_1/SVG	-89.2	7.02×10^{7}	7.846
Cu_1/N_2VG	-256.9	3.77×10^{-32}	-31.423	Pd_1/BVG	91.0	2.23×10^{0}	0.349
Cu_1/C_2N	172.5	1.35×10^{-6}	-5.870	Pd_1/DVG	-153.9	7.35×10^{-3}	-2.134
Cu_1/C_3N_4	157.9	1.08×10^{-9}	-8.967	Pd_1/C_3N_4	16.7	1.66×10^{4}	4.221
Cu_1/GDY	12.3	8.67×10^{3}	3.938	Pd_1/GDY	277.0	2.78×10^{9}	9.444
Cu_2/GDY	115.9	2.61×10^{-1}	-0.583	Pd_2/GDY	-44.8	1.20×10^{8}	8.080
Cu_3/GDY	267.3	6.89×10^{-12}	-11.162	Pd_3/GDY	-68.7	1.23×10^{11}	11.091
Cu_4/GDY	-104.6	1.81×10^{-10}	-9.742	Pd_4/GDY	40.1	8.81×10^{7}	7.945
Cu_7/GDY	64.3	1.81×10^{-18}	-17.743	Pd_7/GDY	57.8	2.91×10^{-1}	-0.536
Cu_{13}/GDY	-42.4	1.51×10^{-20}	-19.802	Pd_{13}/GDY	-56.4	2.81×10^{-6}	-5.551
Cu_{38}/GDY	123.4	3.42×10^{-14}	-13.466	Pd_{38}/GDY	45.9	5.23×10^{-14}	-13.282
Cu_{55}/GDY	188.2	6.73×10^{-11}	-10.172	Pd_{55}/GDY	27.1	1.43×10^{-9}	-8.84

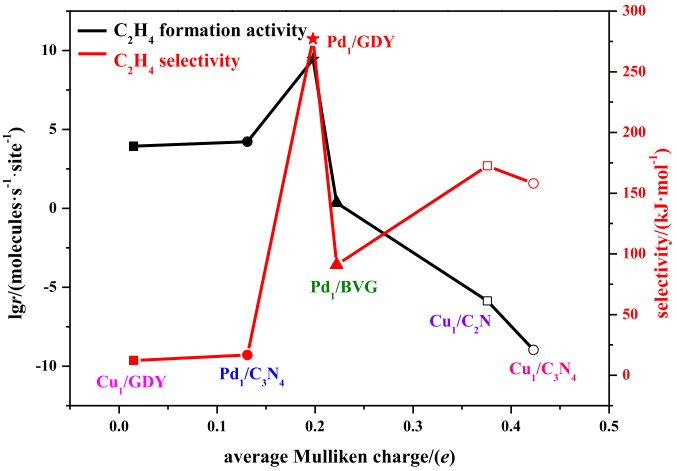

Fig. 6. The relationship of C_2H_4 selectivity and its formation activity with the Mulliken charge (*e*) of metal atoms on the different carbon material supported Cu and Pd single-atom catalysts.

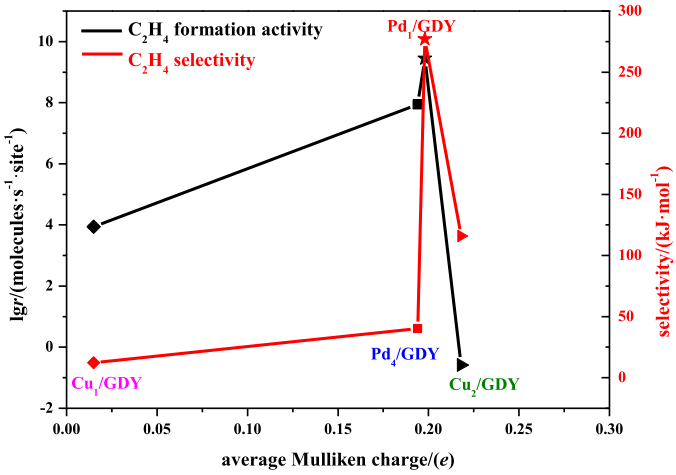

Fig. 7. The relationship of C_2H_4 selectivity and its formation activity with the average Mulliken charge (*e*) of metal atoms on the supported M_n/GDY (M=Cu, Pd, n=1,2,4) catalysts.

kJ•mol^{-1}) and better activity (2.61 × 10^{-1} molecules•s^{-1}•site^{-1}).

For the supported Pd_n/GDY catalysts, C_2H_4 selectivity is Pd_1/GDY>Pd_7/GDY> Pd_{38}/GDY>Pd_4/GDY>Pd_{55}/GDY>Pd_2/GDY>Pd_{13}/GDY>Pd_3/GDY, and the activity is Pd_3/GDY>Pd_1/GDY>Pd_2/GDY>Pd_4/GDY>Pd_7/GDY>Pd_{13}/GDY>Pd_{55}/GDY>Pd_{38}/GDY. The activity of C_2H_4 formation generally decreases with the increase of cluster sizes, while C_2H_4 selectivity does not depend on the cluster sizes. Among them, Pd_1/GDY has both outstanding C_2H_4 selectivity (277.0 kJ•mol^{-1}) and activity (2.78 × 10^9 molecules•s^{-1}•site^{-1}); Pd_4/GDY also shows better C_2H_4 selectivity of 40.1 kJ•mol^{-1} and the activity of 8.81 × 10^7 molecules•s^{-1}•site^{-1}.

In general, C_2H_4 formation activity on Pd_n/GDY is much higher than that on Cu_n/GDY, whereas C_2H_4 selectivity on Cu_n/GDY is better than that on Pd_n/GDY. Further, as listed in Table 2, the cluster size affects the adsorption strength of C_2H_2 and C_2H_4, correspondingly, the adsorption free energy generally increases and then decreases with the change of cluster size; thus, the change of C_2H_4 adsorption free energy alters C_2H_4 desorption ability to affect C_2H_4 selectivity, and the change of C_2H_2 adsorption free energy alters C_2H_2 activation ability to affect C_2H_2 semi-hydrogenation activity, namely, the reaction rate depends on the cluster size.

3.4.3. *Electronic properties of the supported M_n/GDY catalysts*

On above four kinds of Cu_1/GDY, Cu_2/GDY, Pd_1/GDY and Pd_4/GDY screened out with better catalytic performance toward gaseous C_2H_4 formation, the average Mulliken charge of metal atoms is 0.015, 0.218, 0.198 and 0.194 *e*, respectively. As shown in Fig. 7, the relationship of average Mulliken charge with C_2H_4 selectivity and its formation activity (lg*r*) show a quasi-volcanic curve. Cu_1/GDY (0.015 *e*) and Pd_4/GDY (0.194 *e*) with less charge show poor C_2H_4 formation activity (3.938 and 7.945 molecules•s^{-1}•site^{-1}); Cu_2/GDY (0.222 *e*) with more charge exhibits the worst C_2H_4 formation activity (-0.583 molecules•s^{-1}•site^{-1}). However, Pd_1/GDY (0.198 *e*) with moderate charge exhibits the best C_2H_4 formation activity (9.444 molecules•s^{-1}•site^{-1}) and the excellent C_2H_4 selectivity (277.0 kJ•mol^{-1}).

4. Conclusions

DFT calculations are employed to identify the catalytic performance of C_2H_2 semi-hydrogenation on the different carbon material supported M_n (M=Cu, Pd) cluster catalysts with different sizes, aiming at obtaining the influences of support type and cluster size on C_2H_4 selectivity and its formation activity. Nine kinds of the carbon material are considered including the single-defect graphene, double-defect graphene, B-doped graphene, N_1-doped graphene, N_2-doped graphene, N_3-doped graphene, g-C_2N, g-C_3N_4 and GDY. Different carbon material supported single-atom Cu or Pd catalysts were constructed to present the influence of support type, among them, the most suitable carbon material support with the best performance, GDY, was obtained; Further, M_n/GDY (M=Cu, Pd) catalysts were applied to present the influence of metal cluster size, indicating that the activity generally shows a decreasing trend with the increasing of cluster sizes. The analysis of electronic properties unveiled that the best catalytic performance of Pd_1/GDY toward C_2H_2 semi-hydrogenation is ascribed to the moderate Mulliken charge of metal atom. In general, the activity of Pd_n/GDY is better than that of Cu_n/GDY; while the selectivity of Cu_n/GDY is better than that of Pd_n/GDY. Thus, adjusting the support type and cluster size of the carbon material supported metal cluster catalysts is one of the effective method to improve the catalytic performance of C_2H_2 semi-hydrogenation to gaseous C_2H_4 formation.

CRediT authorship contribution statement

Yamin Qi: Writing – original draft, Writing – review & editing, Formal analysis. **Xiuxiu Shao:** Writing – original draft, Formal analysis. **Baojun Wang:** Formal analysis, Supervision, Software, Conceptualization. **Lixia Ling:** Formal analysis. **Riguang Zhang:** Writing – original draft, Writing – review & editing, Data curation, Conceptualization, Funding acquisition, Resources, Software, Project administration, Supervision.

Declaration of Competing Interest

The authors declare that they have no known competing financial interests or personal relationships that could have appeared to influence the work reported in this paper.

Acknowledgment

This work is financially supported by the National Natural Science Foundation of China (Nos. 21776193 and 22078221).

Supplementary materials

Supplementary material associated with this article can be found, in the online version, at doi:10.1016/j.mcat.2021.111840.

References

[1] A.N.R. Bos, K.R. Westerterp, Mechanism and kinetics of the selective hydrogenation of ethyne and ethene, Chem. Eng. Process. 32 (1993) 1–7.
[2] N.S. Schbib, M.A. García, C.E. Gígola, A.F. Errazu, Kinetics of front-end acetylene hydrogenation in ethylene production, Ind. Eng. Chem. Res. 35 (1996) 1496–1505.
[3] J. Osswald, R. Giedigkeit, R. Jentoft, M. Armbruster, F. Girgsdies, K. Kovnir, T. Ressler, Y. Grin, R. Schlogl, Palladium-gallium intermetallic compounds for the selective hydrogenation of acetylene: Part I: Preparation and structural investigation under reaction conditions, J. Catal. 258 (2008) 210–218.
[4] A. Sandell, A. Beutler, A. Jaworowski, M. Wiklund, K. Heister, R. Nyholm, J. N. Andersen, Adsorption of acetylene and hydrogen on Pd(111): Formation of a well-ordered ethylidyne overlayer, Surf. Sci. 415 (1998) 411–422.
[5] B. Yang, R. Burch, C. Hardacre, G. Headdock, P. Hu, Influence of surface structures, subsurface carbon and hydrogen, and surface alloying on the activity and selectivity of acetylene hydrogenation on Pd surfaces: a density functional theory study, J. Catal. 305 (2013) 264–276.
[6] S. Leviness, V. Nair, A.H. Weiss, Acetylene hydrogenation selectivity control on $PdCu/Al_2O_3$ catalysts, J. Mol. Catal. 25 (1984) 131–140.
[7] F. Studt, F. Abild-Pedersen, T. Bligaard, R.Z. Sørensen, C.H. Christensen, J. K. Nørskov, Identification of non-precious metal alloy catalysts for selective hydrogenation of acetylene, Science 320 (2008) 1320–1322.
[8] A. Sárkány, O. Geszti, G. Sáfrán, Preparation of Pd_{shell}-Au_{core}/SiO_2 catalyst and catalytic activity for acetylene hydrogenation, Appl. Catal. A: Gen. 350 (2008) 157–163.
[9] N.C. Cheng, S. Stambula, D. Wang, M.N. Banis, J. Liu, A. Riese, B.W. Xiao, R.Y. Li, T.K. Sham, L.M. Liu, G.A. Botton, X.L. Sun, Platinum single-atom and cluster catalysis of the hydrogen evolution reaction, Nat. Commun. 7 (2016) 13638.
[10] H.T. Chung, D.A. Cullen, D. Higgins, B.T. Sneed, E.F. Holby, K.L. More, P. Zelenay, Direct atomic-level insight into the active sites of a high performance PGM-free ORR catalyst, Science 357 (2017) 479–484.
[11] H. Yan, Y. Lin, H. Wu, W.H. Zhang, Z.H. Sun, H. Cheng, W. Liu, C.L. Wang, J.J. Li, X.H. Huang, T. Yao, J.L. Yang, S.Q. Wei, J.L. Lu, Bottom-up precise synthesis of stable platinum dimers on graphene, Nat. Commun. 8 (2017) 1070.
[12] S.Y. Huang, P. Ganesan, S. Park, B.N. Popov, Development of a titanium dioxide-supported platinum catalyst with ultrahigh stability for polymer electrolyte membrane fuel cell applications, J. Am. Chem. Soc. 131 (2009) 13898–13899.
[13] Z. Xi, D.P. Erdosy, A. Mendoza-Garcia, P.N. Duchesne, J. Li, M. Muzzio, Q. Li, P. Zhang, S. Sun, Pd nanoparticles coupled to $WO_{2.72}$ nanorods for enhanced electrochemical oxidation of formic acid, Nano Lett. 17 (2017) 2727–2731.
[14] S.Q. Zhou, L. Shang, Y.X. Zhao, R. Shi, G.I.N. Waterhouse, Y.C. Huang, L.R. Zheng, T.R. Zhang, Pd single-atom catalysts on nitrogen-doped graphene for the highly selective photothermal hydrogenation of acetylene to ethylene, Adv. Mater. 31 (2019) 1900509–1900515.
[15] F. Huang, Y.C. Deng, Y.L. Chen, X.B. Cai, M. Peng, Z.M. Jia, J.L. Xie, D.Q. Xiao, X. D. Wen, N. Wang, Z. Jiang, H.Y. Liu, D. Ma, Anchoring Cu_1 species over nanodiamond graphene for semi-hydrogenation of acetylene, Nat. Commun. 10 (2019) 4431.
[16] H. Yan, X.X. Zhao, N. Guo, Z.Y. Lyu, Y.H. Du, S.B. Xi, R. Guo, C. Chen, Z.X. Chen, W. Liu, C.H. Yao, J. Li, S.J. Pennycook, W. Chen, C.L. Su, C. Zhang, J. Lu, Atomic engineering of high-density isolated Co atoms on graphene with proximal-atom controlled reaction selectivity, Nat. Commun. 9 (2018) 3197.
[17] X.H. Huang, H. Yan, L. Huang, X.H. Zhang, Y. Lin, J.J. Li, Y.J. Xia, Y.F. Ma, Z. H. Sun, S.Q. Wei, J.L. Lu, Toward understanding of the support effect on Pd_1 single-atom-catalyzed hydrogenation reactions, J. Phys. Chem. C 123 (2019) 7922–7930.
[18] H. Yan, H. Cheng, H. Yi, Y. Lin, T. Yao, C.L. Wang, J.J. Li, S.Q. Wei, J.L. Lu, Single-atom Pd_1/Graphene catalyst achieved by atomic layer deposition: Remarkable performance in selective hydrogenation of 1,3-Butadiene, J. Am. Chem. Soc. 137 (2015) 10484–10487.
[19] M.M. Ugeda, I. Brihuega, F. Guineam, J.M. Gómez-Rodrìguez, Missing atom as a source of carbon magnetism, Phys. Rev. Lett. 104 (2010), 096804.
[20] O.V. Yazyev, S.G. Louie, Topological defects in graphene: Dislocations and grain boundaries, Phys. Rev. B 81 (2010), 195420.
[21] K.M. Fair, X.Y. Cui, L. Li, C.C. Shieh, R.K. Zheng, Z.W. Liu, B. Delley, M.J. Fold, S. P. Ringer, C. Stampfl, Hydrogen adsorption capacity of adatoms on double carbon vacancies of graphene: A trend study from first principles, Phys. Rev. B 87 (2013), 014102.
[22] M. Zhou, Y.H. Lu, Y.Q. Cai, C. Zhang, Y.P. Feng, Adsorption of gas molecules on transition metal embedded graphene: A search for high-performance graphenebased catalysts and gas sensors, Nanotechnology 22 (2011) 385–502.
[23] M. Yan, Z.X. Dai, S.N. Chen, L.J. Dong, X.L. Zhang, Y.J. Xu, C.H. Sun, Single-iron supported on defective graphene as efficient catalysts for oxygen reduction reaction, J. Phys. Chem. C 124 (2020) 13283–13290.
[24] B.R. Sathe, X.X. Zou, T. Asefa, Metal-free B-doped graphene with efficient electrocatalytic activity for hydrogen evolution reaction, Catal. Sci. Technol. 4 (2014) 2023–2030.
[25] J.Y. Dai, J.M. Yuan, P. Giannozzi, Gas adsorption on graphene doped with B, N, Al, and S: A theoretical study, Appl. Phys. Lett. 95 (2009), 232105.
[26] X.H. He, Q. He, Y.C. Deng, M. Peng, H.Y. Chen, Y. Zhang, S.Y. Yao, M.T. Zhang, D. Q. Xiao, D. Ma, B.H. Ge, H.B. Ji, A versatile route to fabricate single atom catalysts with high chemoselectivity and regioselectivity in hydrogenation, Nat. Commun. 10 (2019) 3663.
[27] T. Zhang, D. Zhang, X.H. Han, T. Dong, X.W. Guo, C.S. Song, R. Si, W. Liu, Y.F. Liu, Z.K. Zhao, Preassembly strategy to single Cu-N_3 sites inlaid porous hollow carbonitride spheres for selective oxidation of benzene to phenol, J. Am. Chem. Soc. 140 (2018) 16936–16940.
[28] F.Y. Li, X.Y. Liu, Z.F. Chen, 1+1'>2: Heteronuclear biatom catalyst outperforms its homonuclear counterparts for CO oxidation, Small Methods 3 (2019), 1800480.
[29] W.H. Zhong, Y.X. Liu, M.S. Deng, Y.C. Zhang, C.Y. Jia, O.V. Prezhdo, J.Y. Yuan, J. Jiang, C_2N-supported single metal ion catalyst for HCOOH dehydrogenation, J. Mater. Chem. A 6 (2018) 11105–11112.
[30] N.N. Kong, X. Fan, F.F. Liu, L. Wang, H.P. Lin, Y.Y. Li, S.T. Lee, Single vanadium atoms anchored on graphitic carbon nitride as a high-performance catalyst for non-oxidative propane dehydrogenation, ACS Nano 14 (2020) 5772–5779.
[31] X.H. Haung, Y.J. Xia, Y.J. Cao, X.S. Zheng, H.B. Pan, J.F. Zhu, C. Ma, H.W. Wang, J. J. Li, R. You, S.Q. Wei, W.X. Huang, J.L. Lu, Enhancing both selectivity and coking-resistance of a single-atom Pd_1/C_3N_4 catalyst for acetylene hydrogenation, Nano Res. 10 (2017) 1302–1312.
[32] Y. Zhao, M.Y. Zhu, L.H. Kang, The DFT study of single-atom Pd_1/g-C_3N_4 catalyst for selective acetylene hydrogenation reaction, Catal. Lett. 148 (2018) 2992–3002.
[33] Z.S. Lu, S. Li, P. Lv, C.Z. He, D.W. Ma, Z.X. Yang, First principles study on the interfacial properties of NM/graphdiyne (NM=Pd, Pt, Rh and Ir): The implications for NM growing, Appl. Surf. Sci. 360 (2016) 1–7.
[34] D.H. Xing, C.Q. Xu, Y.G. Wang, J. Li, Heterogeneous single-cluster catalysts for selective semihydrogenation of acetylene with graphdiyne-supported triatomic clusters, J. Phys. Chem. C 123 (2019) 10494–10500.
[35] Y. Wang, Y.M. Qi, M.H. Fan, B.J. Wang, L.X. Ling, R.G. Zhang. C2H2 semi-hydrogenation on the PdxMy cluster/graphdiyne catalysts: effects of cluster composition and size on the activity and selectivity. Green Energy Environ.. https://doi.org/10.1016/j.gee.2020.10.020.
[36] W. Ye, S.M. Chen, Y. Lin, L. Yang, S.J. Chen, X.S. Zheng, Z.M. Qi, C.M. Wang, R. Long, J.F. Zhu, P. Gao, L. Song, J. Jiang, Y.J. Xiong, Precisely tuning the number of Fe atoms in clusters on N-doped carbon toward acidic oxygen reduction reaction, Chem 5 (2019) 2865–2878.
[37] M. Boronat, A. Leyva-Perez, A. Corma, Theoretical and experimental insights into the origin of the catalytic activity of subnanometric gold clusters: attempts to predict reactivity with clusters and nanoparticles of gold, Accounts Chem. Res. 47 (2013) 834–844.
[38] Q.M. Bing, W. Liu, W.C. Yi, J.Y. Liu, Ni anchored C_2N monolayers as low-cost and efficient catalysts for hydrogen production from formic acid, J. Power Sources 413 (2019) 399–407.
[39] C.T. Kuo, Y.B. Lu, L. Kovarik, M. Engelbard, A.M. Karim, Structure sensitivity of acetylene semi-hydrogenation on Pt single atoms and subnanometer clusters, ACS Catal 9 (2019) 11030–11041.
[40] H.Y. Ma, G.C. Wang, Selective hydrogenation of acetylene on Pt/TiO_2 (n=1, 2, 4, 8) surfaces: Structure sensitivity analysis, ACS Catal. 10 (2020) 4922–4928.
[41] X.X Shi, Y. Lin, L. Huang, Z.H. Sun, Y. Yang, X.H. Zhou, E. Vovk, X.Y. Liu, X. H. Huang, M. Sun, S.Q. Wei, J.L. Lu, Copper catalysts in semihydrogenation of acetylene: from single atoms to nanoparticles, ACS Catal 10 (2020) 3495–3504.
[42] B. Delley, From molecules to solids with the $DMol^3$ approach, J. Chem. Phys. 113 (2000) 7756–7764.
[43] B. Delley, An all-electron numerical method for solving the local density functional for polyatomic molecules, J. Chem. Phys. 92 (1990) 508–517.
[44] B. Delley, Fast calculation of electrostatics in crystals and large molecules, J. Phys. Chem. 100 (1996) 6107–6110.
[45] S. Grimme, Density functional theory with London dispersion corrections, Wires. Comput. Mol. Sci. 1 (2011) 211–228.
[46] S. Grimme, J. Antony, S. Ehrlich, H. Krieg, A consistent and accurate ab initio parametrization of density functional dispersion correction (DFT-D) for the 94 elements H-Pu, J. Chem. Phy. 132 (2010), 154104.
[47] S. Grimme, S. Ehrlich, L. Goerigk, Effect of the damping function in dispersion corrected density functional theory, J. Comput. Chem. 32 (2011) 1456–1465.
[48] C.G. Zhou, J.P. Wu, A. Nie, R.C. Forrey, A. Tachibana, H.S. Cheng, On the sequential hydrogen dissociative chemisorption on small platinum clusters: a density functional theory study, J. Phys. Chem. C 111 (2007) 12773–12778.
[49] N. Govind, M. Petersen, G. Fitzgerald, D. King-Smith, J. Andzelm, A generalized synchronous transit method for transition state location, Comp. Mater. Sci. 28 (2003) 250–258.
[50] A.J. McCue, C.J. McRitchie, A.M. Shepherd, J.A. Anderson, Cu/Al_2O_3 catalysts modified with Pd for selective acetylene hydrogenation, J. Catal. 319 (2014) 127–135.
[51] B. Bridier, M.A.G. Hevia, N. López, J. Pérez-Ramírez, Permanent alkene selectivity enhancement in copper-catalyzed propyne hydrogenation by temporary CO supply, J. Catal. 278 (2011) 167–172.
[52] M. Armbrüster, K. Kovnir, M. Behrens, D. Teschner, Y. Grin, R. Schloögl, Pd-Ga intermetallic compounds as highly selective semi-hydrogenation catalysts, J. Am. Chem. Soc. 132 (2010) 14745–14747.
[53] A. Borodziński, G.C. Bond, Selective hydrogenation of ethyne in ethene-rich streams on palladium catalysts. Part 1. Effect of changes to the catalyst during reaction, Catal. Rev. 48 (2006) 91–144.
[54] Y.M. Jin, A.K. Datye, E. Rightor, R. Gulotty, W. Waterman, M. Smith, M. Holbrook, J. Maj, J. Blackson, The influence of catalyst restructuring on the selective hydrogenation of acetylene to ethylene, J. Catal. 203 (2001) 292–306.
[55] S.K. Kim, J.H. Lee, I.Y. Ahn, W.J. Kim, S.H. Moon, Evolution of palladium sulfide phases during thermal treatments and consequences for acetylene hydrogenation, J. Catal. 364 (2018) 204–215.
[56] J.T. Wehrli, D.J. Thomas, M.S. Wainwright, D.L. Trimm, N.W. Cant, Reduced foulant formation during the selective hydrogenation of C_2, C_3, and C_4 acetylenes, Stud. Surf. Sci. Catal. 68 (1991) 203–210.
[57] I.Y. Ahn, J.H. Lee, S.S. Kum, S.H. Moon, Formation of C_4 species in the deactivation of a Pd/SiO_2 catalyst during the selective hydrogenation of acetylene, Catal. Today 123 (2007) 151–157.

[58] G.C. Battiston, L. Dalloro, G.R. Tauszik, Performance and aging of catalysts for the selective hydrogenation of acetylene: a micropilot-plant study, Appl. Catal. 2 (1982) 1–17.
[59] L. Yayun, Z. Jing, M. Xueru, Study on the formation of polymers during the hydrogenation of acetylene in ethylene ethane fraction, Proc. Joint Meeting Chem. Eng., Chem. Ind. Eng. Soc. China, AIChE, Beijing. 2 (1982) 688–702.
[60] B. Yang, R. Burch, C. Hardacre, P. Hu, P. Hughes, Mechanistic study of 1, 3-butadiene formation in acetylene hydrogenation over the Pd-based catalysts using density functional calculations, J. Phys. Chem. C 118 (2014) 1560–1567.
[61] M.J. Vincent, R.D. Gonzalez, Selective hydrogenation of acetylene through a short contact time reactor, AIChE J 48 (2004) 1257–1267.
[62] J.B. Zhao, S.J. Zha, R. Mu, Z.J. Zhao, J.L. Gong, Coverage effect on the activity of the acetylene semihydrogenation over Pd-Sn catalysts: A density functional theory study, J. Phys. Chem. C 122 (2018) 6005–6013.